Atmos. Chem. Phys., 16, 14265–14283, 2016
www.atmos-chem-phys.net/16/14265/2016/
doi:10.5194/acp-16-14265-2016

Atmospheric Chemistry and Physics Open Access EGU

Observation of regional air pollutant transport between the megacity Beijing and the North China Plain

Yingruo Li[1], Chunxiang Ye[1,a], Jun Liu[1], Yi Zhu[1], Junxia Wang[1], Ziqiang Tan[1], Weili Lin[2], Limin Zeng[1], and Tong Zhu[1]

[1]SKL-ESPC and BIC-ESAT, College of Environmental Sciences and Engineering, Peking University, Beijing, 100871, China
[2]Meteorological Observation Center, China Meteorological Administration, Beijing, 100081, China
[a]now at: School of Chemistry, University of Leeds, Leeds LS2 9JT, UK

Correspondence to: Tong Zhu (tzhu@pku.edu.cn)

Received: 10 June 2016 – Published in Atmos. Chem. Phys. Discuss.: 13 June 2016
Revised: 18 October 2016 – Accepted: 18 October 2016 – Published: 16 November 2016

Abstract. Megacities have strong interactions with the surrounding regions through transport of air pollutants. It has been frequently addressed that the air quality of Beijing is influenced by the influx of air pollutants from the North China Plain (NCP). Estimations of air pollutant cross-boundary transport between Beijing and the NCP are important for air quality management. However, evaluation of cross-boundary transport using long-term observations is very limited. Using the observational results of the gaseous pollutants SO_2, NO, NO_2, O_3, and CO from August 2006 to October 2008 at the Yufa site, a cross-boundary site between the megacity Beijing and the NCP, together with meteorological parameters, we explored a method for evaluating the transport flux intensities at Yufa, as part of the "Campaign of Air Quality Research in Beijing and Surrounding Region 2006–2008" (CARE-Beijing 2006–2008). The hourly mean ± SD (median) concentration of SO_2, NO, NO_2, NO_x, O_3, O_x, and CO was 15 ± 16 (9) ppb, 12 ± 25 (3) ppb, 24 ± 19 (20) ppb, 36 ± 39 (23) ppb, 28 ± 27 (21) ppb, 52 ± 24 (45) ppb, and 1.6 ± 1.4 (1.2) ppm during the observation period, respectively. The bivariate polar plots showed the dependence of pollutant concentrations on both wind speed and wind direction, and thus inferred their dominant transport directions. Surface flux intensity calculations further demonstrated the regional transport influence of Beijing and the NCP on Yufa. The net surface transport flux intensity (mean ± SD) of SO_2, NO, NO_2, NO_x, O_3, O_x, and CO was 6.2 ± 89.5, -4.3 ± 29.5, -0.6 ± 72.3, -4.9 ± 93.0, 14.7 ± 187.8, 14.8 ± 234.9, and $70 \pm 2830\,\mu g\,s^{-1}\,m^{-2}$ during the observation period, respectively. For SO_2, CO, O_3, and O_x the surface flux intensities from the NCP to Yufa surpassed those from Beijing to Yufa in all seasons except winter, with the strongest net fluxes largely in summer, which were about 4–8 times those of other seasons. The surface transport flux intensity of NO_x from Beijing to Yufa was stronger than that from the NCP to Yufa except in summer, with the strongest net flux in winter, which was about 1.3–8 times that of other seasons. The flux intensities were then assigned to the corresponding trajectories in the potential source contribution function analysis (PSCF), which confirmed the results of flux intensity calculations. Our study also suggested that various factors, such as the wind field, emission inventory, and photochemical reactions, could influence transport of air pollutants. The decrease of surface flux intensity during the Olympic Games implied the role of both local emission reduction and regional cooperation in successful air quality management. Three dimensional observations are needed for further comprehensive discussion of the regional transport between Beijing and the NCP.

1 Introduction

Megacities are large sources of air pollutants and greatly influence the surrounding areas (Parrish and Zhu, 2009). With a population over 20 million, the city of Beijing is an example of such a megacity. Beijing has faced severe air pollution problems over the past two decades and has intensive interactions with other emission hot spots within the North China Plain (NCP) (Chen et al., 2015; Shao et al., 2006; Zhang et

al., 2012). Beijing and the NCP are surrounded by the Yanshan Mountains to the north and the Taihang Mountains to the west. The semi-basin geographical features together with the continental monsoon climate make regional transport of air pollutants between the megacity Beijing and the NCP an important factor affecting air quality in Beijing and the NCP (An et al., 2007; Guo et al., 2010; Lin et al., 2008, 2009; Streets et al., 2007; Wang et al., 2006, 2011, 2015; Wu et al., 2011; Xu et al., 2005, 2011). An improved understanding of the regional transport of air pollutants between Beijing and the NCP is therefore essential for air quality management of the megacity Beijing and establishment of regional-scale emissions control measures.

Previous studies have shed light on the regional transport sources of the megacity Beijing, and various techniques have been employed, including rural–urban station observations (Guo et al., 2010; Lin et al., 2008, 2009; Wang et al., 2006; Xu et al., 2011), mobile laboratory measurements (Wang et al., 2009a, 2011; Zhu et al., 2016), and modeling studies (An et al., 2007; Matsui et al., 2009; Wu et al., 2011). A ground-based observation study from July 2006 to September 2007 at the Gucheng site (Lin et al., 2009), a rural site southwest of Beijing, found that high concentrations of gaseous pollutants, including nitric oxide (NO), nitrogen dioxide (NO_2), nitrogen oxides ($NO_x = NO + NO_2$), sulphur dioxide (SO_2), carbon monoxide (CO), ozone (O_3), and oxidant ($O_x = NO_2 + O_3$), were accompanied by air masses moving northward from Gucheng to Beijing, according to back-trajectory analysis. Similar to Lin et al. (2009), regional transport of air pollutants between Beijing and the NCP was observed consistently in previous studies (Lin et al., 2008; Yuan et al., 2009; Zhu et al., 2011), even though they were merely short-term observations.

Many studies have also attempted to quantify transport fluxes of the main gaseous pollutants. A mobile laboratory study in Beijing demonstrated regional transport of SO_2 from the NCP in both emission-control and non-control scenarios during the Beijing 2008 Olympics (Wang et al., 2011). Extrapolated from five 1-day case studies, the annual transport fluxes of SO_2 from the southeastern part of the 6th Ring Road into Beijing were estimated at 49.2 and 146.3 Gg yr^{-1}, accounting for 70 and 73 % of the annual SO_2 emissions in Beijing under emission-control and non-control scenarios, respectively. The Community Multi-scale Air Quality (CMAQ) model simulation by An et al. (2007) found that regional transport from the surrounding areas of Beijing contributed 39 % of $PM_{2.5}$, 30 % of PM_{10}, and 18 % of SO_2 to the city on average in a heavy pollution episode in the spring of 2005. Similarly, the CMAQ model simulation over the Beijing region for July 2001, reported by Streets et al. (2007), illustrated the regional transport of $PM_{2.5}$ and O_3 between Beijing and the NCP. The study suggested that the average contributions of regional transport to $PM_{2.5}$ concentrations in the megacity Beijing from Hebei Province, Shandong Province, and Shanxi Province were about 32, 11, and 3.5 %, with maximum contributions of 70, 63, and 21 %, respectively. The regional transport contributions to the concentrations of O_3 in Beijing were less significant, with maximum contributions of 28 % from Hebei Province, 24 % from Shandong Province, and 10 % from Shanxi Province.

In summary, long-term observation of transport flux is necessary to constrain regional models and to directly evaluate the influence of regional transport on air quality. Estimations of air pollutant cross-boundary transport between Beijing and the NCP are important for air quality management. However, evaluation of cross-boundary transport using long-term observations is very limited. In this study, we developed a method of calculating the surface transport flux intensity across a cross-boundary site based on long-term ground-based measurement and evaluated the regional transport influence of Beijing and the NCP on the cross-boundary site. The results showed different transport directions and seasonal variations in the surface transport flux intensities of the main pollutants, including SO_2, NO, NO_2, NO_x, O_3, and CO, at the Yufa site. The key factors controlling regional transport are also discussed, which is important for the establishment of air quality control policy in the future.

2 Measurements and methods

2.1 Measurements

The Yufa site is located at the cross-boundary area between Beijing and the NCP and could be influenced by emissions from the megacity Beijing and long-range transport from the NCP. The measurements at the Yufa site (39°30′49″ N, 116°18′15″ E) were conducted on the top of a building (about 20 m above ground level) on the campus of Huangpu College. There is no tall building that affects the wind and gaseous pollutant measurements around the Yufa site. This is a rural site about 50 km south of the center of Beijing and near the border of Beijing Municipality and Hebei Province. As shown in Fig. 1, the Yufa site is located in the temperate monsoon climate zone and the topography of its surrounding area is flat. The prevailing wind of the Yufa site is the same as the surrounding region (Lin et al., 2009); thus, the wind field of the Yufa site is representative of the researched area in this study. The northern and western sides of the site are mountain areas where dry and clean air masses come from, whereas the southern and southeastern sides are surrounded by heavily industrialized and urbanized areas, such as Hebei Province and Tianjin City (Fig. 1).

The gaseous pollutant species measured included SO_2, NO, NO_2, NO_x, O_3, and CO. SO_2 was measured using a sulphur dioxide analyzer (9850B; Ecotech, Knoxfield, Australia), which combines microprocessor control with pulsed UV fluorescence detection with a precision of 0.5 ppb and an uncertainty within 10 %. The detection limit for the analyzer is 0.5 ppb and the time resolution is 1 min. Reactive nitrogen

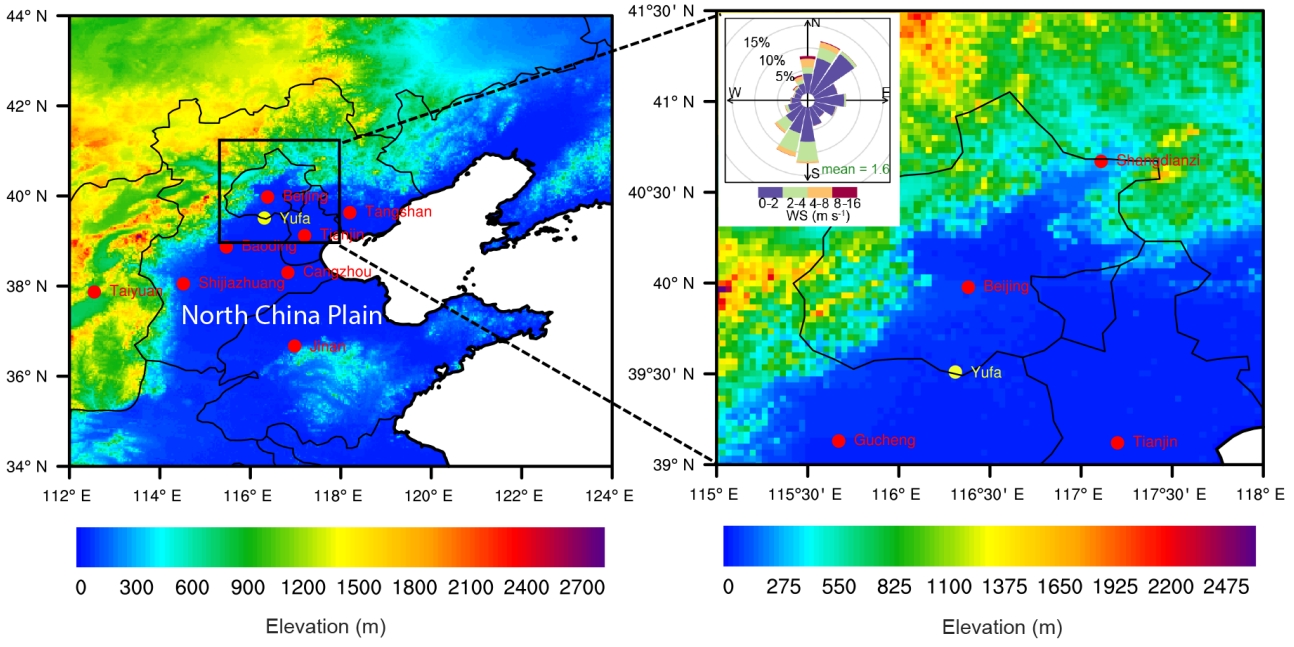

Figure 1. The location information of the Yufa site.

species (NO, NO_2, and NO_x) were measured using nitrogen analyzer (9841B; Ecotech), which utilizes microprocessor control and chemiluminescence detection with a precision of 0.5 ppb and an uncertainty within 10 %. The detection limit for the instrument is 0.5 ppb and the time resolution is 1 min. CO was measured using a CO analyzer (9830A; Ecotech), which utilizes nondispersive infrared (NDIR) gas filter correlation photometry and microprocessor control with a precision of 0.1 ppm and an uncertainty within 1 %. The detection limit for the instrument is 50 ppb and the time resolution is 1 min. O_3 was measured using an ozone analyzer (9810B; Ecotech), which combines microprocessor control with UV photometry with a precision of 1 ppb and an uncertainty within 5 %. The detection limit for the instrument is 0.4 ppb and the time resolution is 1 min. Measurements of meteorological parameters, including wind direction (WD), wind speed (WS), temperature (T), barometric pressure (BP), and relative humidity (RH), were conducted with a LSI LASTEM auto meteorology station (LSI LASTEM; Milan, Italy). All trace gas instruments were maintained and calibrated routinely following the manufacturer's protocols. The main reasons for missing data were power and instrument failure. The detailed information of the instruments is listed in Table 1.

2.2 Methods

2.2.1 Transport direction analysis

The transport of gaseous pollutants is markedly influenced by meteorological parameters, especially wind speed and wind direction. For local emission sources, wind can facilitate the dilution and diffusion of air pollutants. Strong wind usually has marked diffusion capability, whereas weak wind usually leads to accumulation of air pollutants. For regional sources, strong wind can transport pollutants over long distances and may result in high concentrations of pollutants in downwind areas. Therefore, the relationship between pollutant concentration and wind field is an indicator of regional transport.

The bivariate polar plot graphical technique was used to investigate the relationships between the concentrations of gaseous pollutants and wind field and to identify potential emissions sources and transport directions of air pollutants according to the technique developed by Carslaw et al. (2006) and Westmoreland et al. (2007). The variables (such as pollutant concentrations, wind speed, and wind direction) were plotted in polar coordinates. The procedure was as follows. First, the concentration data were partitioned into wind speed–wind direction bins, and the mean concentrations were calculated within each bin. Then, the wind components u and v were calculated using Eq. (1):

$$u = \mathrm{WS} \times \sin(\pi\theta/180),\ v = \mathrm{WS} \times \cos(\pi\theta/180), \quad (1)$$

where WS is the hourly mean wind speed, and θ is the wind direction in degrees, with 90° being from the east. Then, a generalized additive model (GAM; Jayamurugan et al., 2013) was used for surface fitting to describe the concentration as a function of the wind components u and v. The concentrations calculated by the GAM can be expressed with Eq. (2):

$$\sqrt{C_i} = \beta_0 + s\,(u, v) + e_i\,(2), \quad (2)$$

Table 1. The overview of measurement instruments.

Species/ parameter	Instrument	Detection limit	Time resolution	Precision	Uncertainty
SO_2	Ecotech 9850B	0.5 ppb	1 min	0.5 % (0.5 ppb)	10 %
NO–NO_x	Ecotech 9841B	0.5 ppb	1 min	1 % (0.5 ppb)	10 %
CO	Ecotech 9830	50 ppb	1 min	1 % (0.1 ppm)	1 %
O_3	Ecotech 9810B	0.4 ppb	1 min	0.5 % (1 ppb)	5 %
WS	LSI LASTEM	–	10 min	0.1 m s^{-1}	5 %
WD	LSI LASTEM	–	10 min	0.1°	1 %
BP	LSI LASTEM	–	10 min	0.1 hPa	±0.35 hPa
T	LSI LASTEM	–	10 min	0.1 °C	±0.2 °C
RH	LSI LASTEM	–	10 min	1 %	±3 %

where C_i is the calculated pollutant concentration, β_0 is the overall mean of the response, $s(u, v)$ is the smooth function, and e_i is the residual.

Compared to the nonparametric regression used by Henry et al. (2002), the bivariate polar plot involves the dependence of pollutant concentration on both wind speed and wind direction. The nonlinear relationships among the variables (such as concentrations of gaseous pollutants, wind speed, and wind direction) as well as the interactions among these variables can be considered using the GAM method for data smoothing. In addition, the use of polar coordinates makes the graphics more intuitive.

2.2.2 Transport flux assessment

The surface transport fluxes at the Yufa site were calculated with the following formula (White et al., 1976; Wang et al., 2011):

$$f = -\frac{1}{n}\sum_{j=1}^{n} C_j \times \mathrm{WS}_j \times \cos\theta_j, \quad (3)$$

$$\sigma = H_0 \times L_0, \quad (4)$$

$$\mathrm{FLUX} = f \times \sigma, \quad (5)$$

where f is surface flux intensity of the pollutants, i.e., the per unit area flux (μg s^{-1} m^{-2}); C_j is the mean concentration of the pollutants (μg m^{-3}) during the jth observation hour; θ_j is the angle between wind direction and the north–south direction during the jth observation hour; WS_j is wind speed (m s^{-1}) during the jth observation hour; n is the total number of observation hours; and σ is the surface cross-sectional area (m^2) with a width of L_0 (m) and a height of H_0 (m). The average surface flux of the pollutants (i.e., FLUX, μg s^{-1}) can be obtained by multiplying flux intensity f and the cross-section area σ.

Figure S1 in the Supplement shows a schematic diagram of the surface flux calculation. The flux intensity here is the product of wind vector and air pollutant concentration measured at the same location. Ideally, we need to use the wind speed and air pollutant concentration with infinite small time resolution to conduct the surface flux calculations. In this study, the hourly data of the pollutants and wind were used, mainly because the pollutant concentration data were converted from the minute data to hourly mean to remove accidental fluctuation and reduce noise. Therefore, we assumed the wind speed and wind direction were constant within 1 h, and hourly wind data were used to match with the hourly air pollutant concentration data to calculate the flux intensity.

It must also be made clear that the surface flux intensity calculated in this study is the per unit area flux across the Yufa site, which is different from the flux across a large area reported in other studies (e.g., Wang et al., 2011). Our results could only be extrapolated if the concentrations of all the pollutants, and wind speed and direction were homogenously distributed, vertically and horizontally. Otherwise, vertical profiles of air pollutant concentration and wind are needed to calculate the cross-section transport flux of two adjacent regions for the whole boundary layer with the integrating formula below:

$$\begin{aligned}\mathrm{FLUX} &= \int\int C_{(x,z)}\mathrm{WS}_{(x,z)}\sin\theta_{(x,z)}\mathrm{d}x\mathrm{d}z \\ &= \int\int f_{(x,z)}\mathrm{d}x\mathrm{d}z, \end{aligned} \quad (6)$$

where x is horizontal distance to the observed point and z is the vertical distance from ground to the observed point. In this study, we focus on developing the method that uses surface flux intensity calculation and evaluation of the regional transport influence of Beijing and the NCP on the cross-boundary site based on the ground-based observation data.

2.2.3 The backward trajectory model and PSCF analysis

The 12 h air mass back trajectories arriving at the Yufa site at 500 m above ground level were calculated using the National Oceanic and Atmospheric Administration (NOAA) Hybrid Single-Particle Lagrangian Integrated Trajectory Version 4 model (HYSPLIT-4 model)

(http://ready.arl.noaa.gov/HYSPLIT.php) during the study period (from 15 August 2006 to 31 October 2008) with a $1^\circ \times 1^\circ$ latitude–longitude horizontal resolution and the final meteorological database. The final archived meteorological data were obtained from the National Centers for Environmental Prediction's (NCEP's) Global Data Assimilation System (GDAS) (ftp://arlftp.arlhq.noaa.gov/pub/archives/gdas1). The back trajectories were generated with 6 h time resolution (four times per day) at starting times of 00:00, 06:00, 12:00, and 18:00 UTC (08:00, 14:00, 20:00, 04:00 LT (local time), respectively).

The potential source contribution function (PSCF) analysis was performed with the GIS-based software TrajStat (http://www.meteothinker.com/products/trajstat.html) (Wang et al., 2009b). The PSCF analysis has been widely used for identifying the possible source areas of the observed high concentrations of pollutants at the receptor site (Ashbaugh et al., 1985; Zhang et al., 2013). In this study the long-term calculated surface flux intensity data were assigned to the backward trajectories in the PSCF analysis to confirm the bidirectional transport of pollutants between Beijing and the NCP. The PSCF analysis was conducted as follows.

The study domain was divided into $i \times j$ equal size grid cells and the PSCF value for the ijth cell is defined as

$$\mathrm{PSCF}_{ij} = m_{ij}/Mn_{ij}, \tag{7}$$

where n_{ij} denotes the number of endpoints that fall in the ijth cell and m_{ij} represents the number of endpoints for the same cell having arrival times at the observed site corresponding to measured data higher than an arbitrarily set criterion.

To reduce the effect of small values of n_{ij}, the PSCF values were multiplied by an arbitrary weigh function W_{ij}. In this study, W_{ij} is defined as below.

$$W_{ij} = \begin{cases} 1.00, & 80 < n_{ij} \\ 0.70, & 20 < n_{ij} \le 80 \\ 0.42, & 10 < n_{ij} \le 20 \\ 0.05, & n_{ij} \le 10 \end{cases} \tag{8}$$

In this study, the study domain was 30–50° N, 100–125° E and the horizontal resolution was $0.25^\circ \times 0.25^\circ$.

3 Results and discussion

3.1 Observations

The time series of hourly average and 24 h smoothing concentrations of SO_2, NO, NO_2, NO_x, O_3, O_x, and CO observed at the Yufa site from 15 August 2006 to 31 October 2008 are shown in Fig. 2. The hourly mean ± SD (median) concentration values of SO_2, NO, NO_2, NO_x, O_3, O_x, and CO were 15 ± 16 (9) ppb, 12 ± 25 (3) ppb, 24 ± 19 (20) ppb, 36 ± 39 (23), 28 ± 27 (21) ppb, 52 ± 24 (45) ppb, and 1.6 ± 1.4 (1.2) ppm during the observation period from 1 September 2006 to 31 August 2008, respectively, with hourly mean values −3, 1, 6, 7, −1, 5, and 0 ppb higher for SO_2, NO, NO_2, NO_x, O_3, O_x, and CO, respectively, than the Gucheng site, a polluted rural site to the southwest of Beijing, from July 2006 to September 2007 (Lin et al., 2009). The hourly mean values were 12, 11, 17, 28, −5, 22, and 972 ppb higher than those observed at the clean background at the Shangdianzi site, which is one of the regional Global Atmosphere Watch (GAW) stations in China over the period 2004–2006 (Lin et al., 2008). The compared results indicated that the Yufa site has become a relatively polluted rural site. Typical seasonal variations were observed for all gaseous pollutants. Concentrations of primary pollutants, including SO_2, NO, NO_2, NO_x, and CO, were high in winter and low in summer. In contrast, the concentration of O_3, which is a secondary pollutant, was high in summer and low in winter.

Meteorological parameters such as WS, WD, RH, T, and BP were also measured at the Yufa site; the monthly statistics are shown in Fig. 3. Northern (usually in winter) or southern wind (usually in summer) prevailed at the Yufa site, with monthly average wind speed mostly below $2\,\mathrm{m\,s^{-1}}$. Exceptional conditions occurred occasionally in spring and winter for the northern wind, with monthly average wind speeds around $2–3\,\mathrm{m\,s^{-1}}$. In addition, for the northern wind, the mean speed was higher than the median speed, suggesting the prevalence of high wind speeds in both spring and winter. Prevailing northern wind with high wind speed during winter and spring has been reported consistently in the Beijing area (Lin et al., 2008; Wehner et al., 2008). Another exceptional condition occurred in spring for the southern wind, with a monthly average wind speed around $2\,\mathrm{m\,s^{-1}}$. Figure 4 summarizes the prevalence of wind direction in the four seasons. Generally, the prevailing surface wind directions were north-northeast and south-southwest in all seasons. In winter and spring, winds from the north-northeast sector made a contribution of about 40–50 % to wind frequency. Whereas under the influence of summer monsoons, winds from the south increased significantly in summer, with the contribution to wind frequency above 40 %. RH was higher in summer and lower in spring and winter with the driest month in April of 2007 and February of 2008. The seasonal variation in RH may partially be related to the variations in WS (Lin et al., 2011). T was higher in summer and lower in winter. Surface pressure measurements showed high values in winter and low values in summer due to surface heating and lifting air masses in summer, which partly accounted for the wind field in the NCP (Takegawa et al., 2009).

The seasonal variations in gaseous pollutants and meteorological parameters could be linked in certain ways. For example, the high temperature and low pressure in summer suggested a high boundary layer and diluted gaseous pollutants to some extent. The high temperature, light intensity, and relative humidity also favored the chemical transforma-

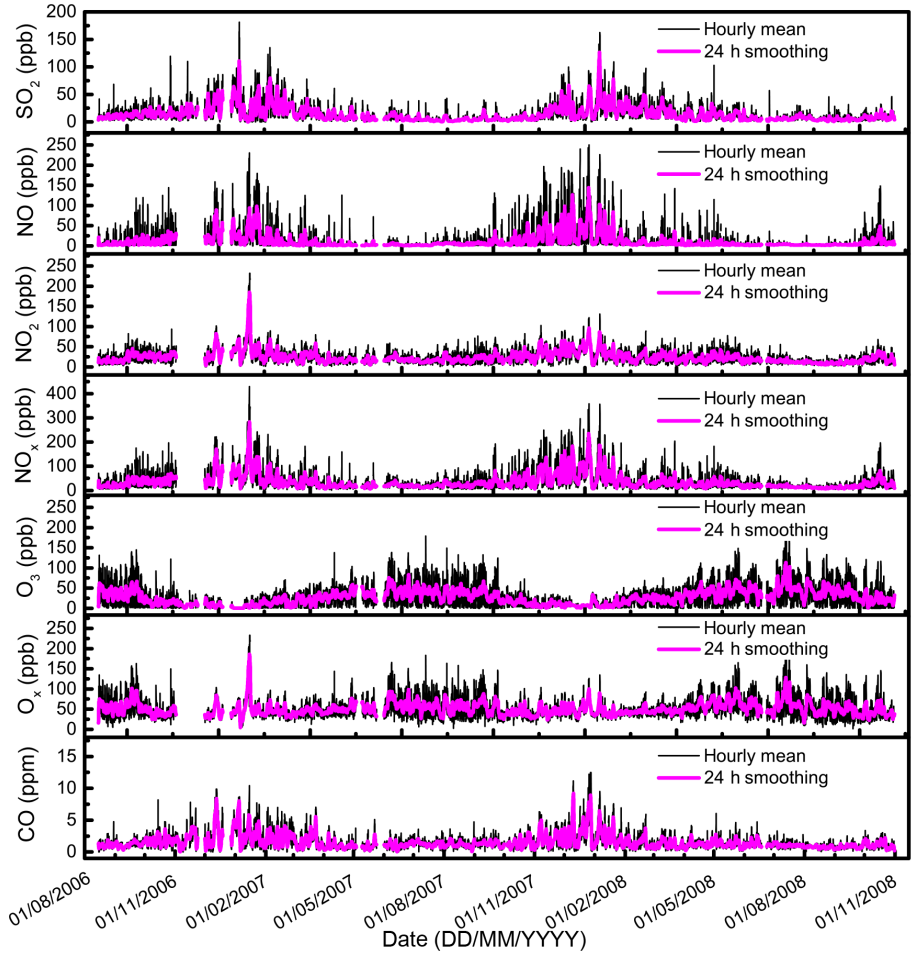

Figure 2. Time series of hourly mean (black line) and 24 h smoothing concentrations (red line) of SO_2, NO, NO_2, NO_x, O_3, O_x, and CO at the Yufa site from 15 August 2006 to 31 October 2008.

tion of these primary pollutants and the formation of secondary pollutants. The high wind speeds in spring and winter also affected regional transport, and therefore the concentrations of gaseous pollutants, as discussed below.

3.2 Transport direction

3.2.1 The bivariate polar plots for the whole observed period

As shown in Fig. 1, the Yufa site is located in the boundary area of Beijing city and the NCP. Prevalent south-southwestern or north-northeastern wind would bring in polluted or clean air masses to the site. Air masses from both directions would pass over the Yufa site. Regional transport from the megacity Beijing and the NCP could therefore be observed at the Yufa site. The transport directions for gaseous pollutants, including SO_2, NO, NO_2, NO_x, O_3, O_x, and CO, will be discussed in this section.

Figure 5a–g show the bivariate polar plots for SO_2, NO, NO_2, NO_x, O_3, O_x, and CO at the Yufa site, respectively. In the low wind speed scenario, high or medium concentrations of NO, NO_2, NO_x, SO_2, and CO were generally observed, along with low O_3 and O_x concentrations. In the high wind speed scenario, the dependence of species concentration on wind speed and wind direction was more varied. Specifically, the bivariate polar plot in Fig. 5b clearly shows dependence of high NO concentration (higher than 30 ppb) on low wind speed, with low NO concentration (lower than 5 ppb) at wind speeds $>3\,m\,s^{-1}$. The bivariate polar plot in Fig. 5c shows similar dependence of high NO_2 concentration on low wind speed, but NO_2 concentrations up to 20 ppb were still observed with medium wind speeds of around $5\,m\,s^{-1}$ from the south, east, and northeast. Accordingly, the dependence pattern of the NO_x concentration (Fig. 5d) on wind speed and wind direction reflected the features of both NO and NO_2. The dependence pattern of high CO concentration on low wind speed in Fig. 5g was similar to that for NO_x, but a considerable CO concentration, substantially higher than

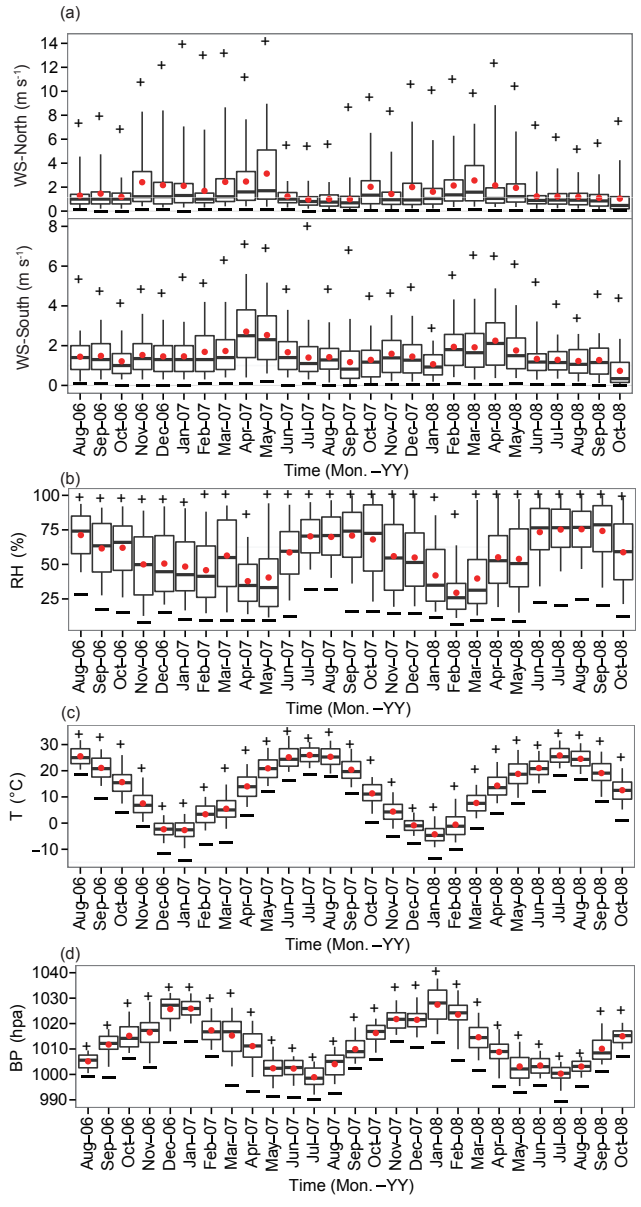

Figure 3. Monthly statistics of wind speed (WS) for northern wind **(a)** top and southern wind **(a)** bottom, relative humidity (RH) **(b)**, temperature (T) **(c)**, and barometric pressure (BP) **(d)** at the Yufa site. The red point represents the mean value. The black cross bar stands for the median value. The black box and whisker denote the 5th, 25th, 75th, and 95th percentiles. The plus and minus symbols represent the maximum and minimum, respectively. It should be clarified that the northern and southern winds here are different from the wind direction definition in meteorology. The southern wind here is the wind with direction from 90–270°, while the northern wind is from 0–90° and from 270–360°.

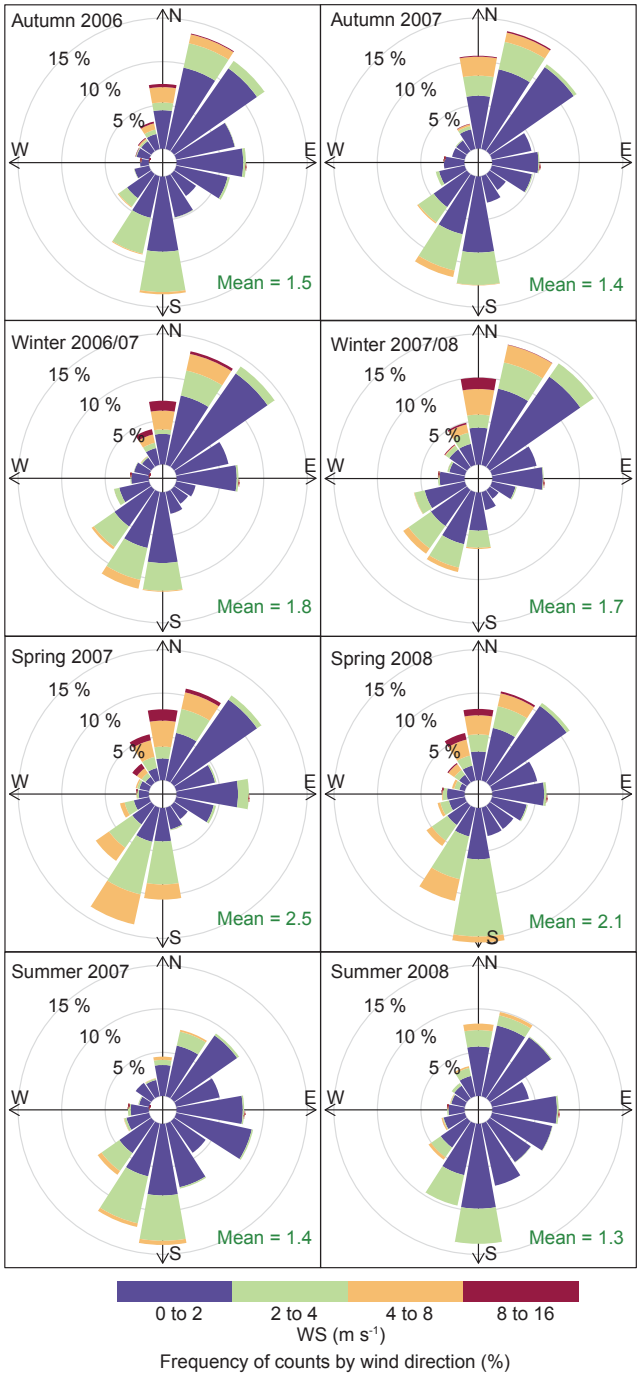

Figure 4. Wind rose plots based on frequencies of hourly data in Autumn 2006, Autumn 2007, Winter 2006/07, Winter 2007/08, Spring 2007, Spring 2008, Summer 2007, Summer 2008. Spring (MAM): March, April, and May; Summer (JJA): June, July, and August; Autumn (SON): September, October, and November; Winter (DJF): December, January, and February.

background level, was still observed at wind speeds exceeding $5\,m\,s^{-1}$ from the south and the east. Figure 5a shows similar dependence of medium–high concentration of SO_2 (>15 ppb) on low wind speed, with one unique feature being that high SO_2 concentration was observed under conditions of high wind speed ($>5\,m\,s^{-1}$) in various wind directions (especially the southern wind). Finally, the bivariate

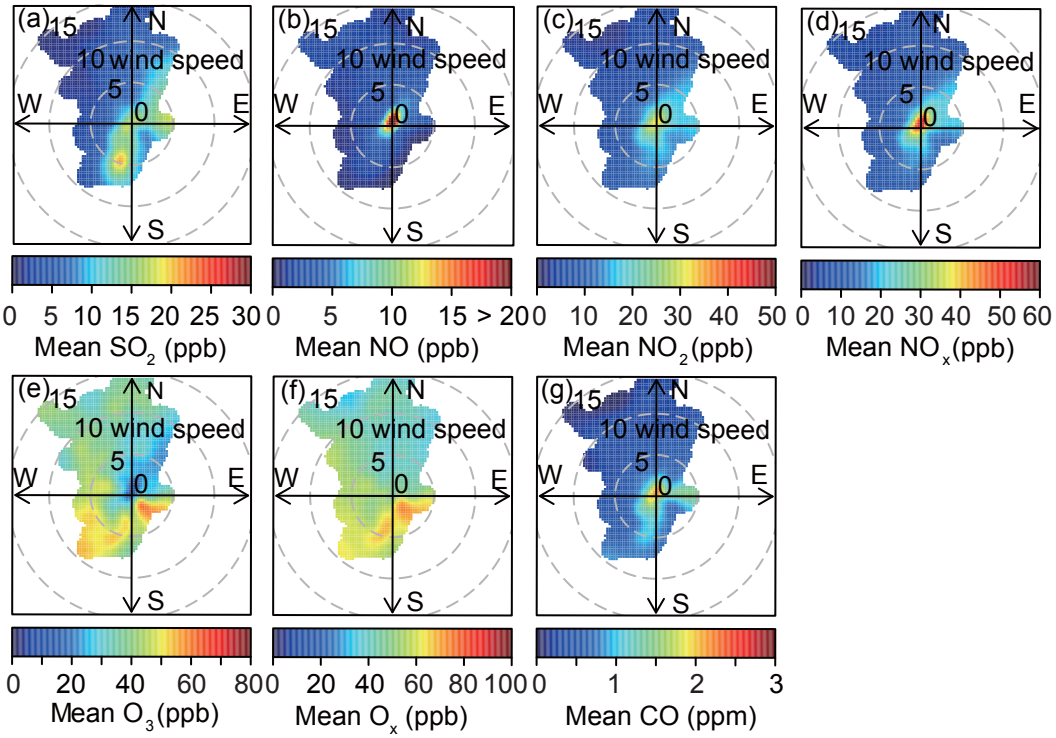

Figure 5. Bivariate polar plots for SO_2 **(a)**, NO **(b)**, NO_2 **(c)**, NO_x **(d)**, O_3 **(e)**, O_x **(f)**, and CO **(g)** concentrations based on hourly average data at the Yufa site from 1 September 2006 to 31 August 2008. The color scale shows the concentrations of pollutants in ppb (or ppm specially for CO), and the radial scale shows the wind speed ($m\,s^{-1}$), which increases from the center of the plot radially outwards.

polar plot in Fig. 5e shows the dependence of O_3 concentration on wind speed and wind direction, which was somewhat opposite to the patterns for other species. The low O_3 concentration (< 20 ppb) was related to low wind speed or calm wind conditions. With the northern wind and medium or high wind speed, a typical background O_3 concentration (around 50 ppb) was observed. With southern wind and medium or high wind speed, high O_3 concentration was observed. The dependence of the high O_x concentration on high wind speed from the south and southeast was similar to that of O_3, but no low concentration of O_x was observed under low wind speed conditions (Fig. 5f), probably due to the compensation of high NO_x concentration at low wind speeds (Fig. 5d).

The high concentrations of NO, NO_2, NO_x, and CO and the medium-high concentration of SO_2 observed under low wind speed conditions were consistent with their high emission intensities in the Beijing area (Fig. 6). Due to the marked increase in the number of vehicles and heavy energy consumption, Beijing has been a well-known emission hot spot for NO and NO_2 (Tang, 2004). Meanwhile, the extremely high levels of CO emissions in the Beijing area are clearly shown in the emissions map (Fig. 6) and have been reported consistently (Wang et al., 2009a) and directly observed with peak CO concentrations of up to 9.3 ppm. Only medium-high SO_2 concentration (> 15 ppb) observed even at low wind speed suggested the successful reduction of SO_2 emission, which could be ascribed to the continuous effort of the Chinese government since the 1990s and during the Olympic Games (Qin et al., 2009; Tang, 2004; Wang et al., 2009a, 2011). Accordingly, the O_3 concentration under low wind speed conditions was lower than the typical background level, which could be attributed to the rapid titration of O_3 by accumulation of NO.

3.2.2 Seasonal variations of the bivariate polar plots

The different patterns of the bivariate polar plots reflected the differences in local emission and regional transport for different species. The emissions, the meteorological conditions, the chemical reaction rate, and the species lifetime, which have essential influence on the regional transport, vary greatly by seasons. Thus the seasonal variations of the bivariate polar plots and the corresponding causes were discussed in this section.

Figure 7b–d show seasonal variations of the bivariate polar plots for NO, NO_2, and NO_x at the Yufa site, respectively. Generally, the mean concentrations of NO_2, NO_x and especially NO in the low wind speed scenario were higher than those in the higher wind speed scenario in all seasons. The mean concentration of NO was less than 10 ppb when the wind speed higher was than $5\,m\,s^{-1}$ in all seasons (Fig. 7b). Figure 7c clearly shows the relatively higher con-

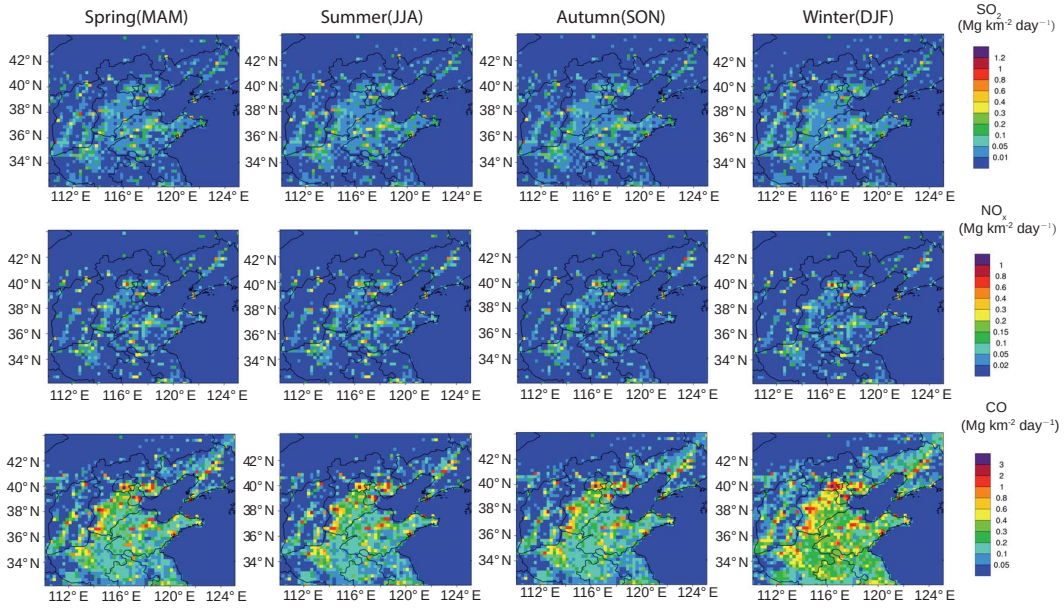

Figure 6. Spatial distribution of seasonal NO_x, CO, and SO_2 emissions in 2008 based on the Multi-resolution Emission Inventory for China (MEIC; www.meicmodel.org) (unit: Mg km^{-2} d^{-1}, horizontal resolution: 25 km × 25 km).

centration of NO_2 (∼ 20 ppb) with winds at a higher wind speed (> 5 m s^{-1}) from the southern sector in spring, from the northeastern and southern sectors in summer and winter, and from the northeastern sector in autumn. Figure 7d shows that the dependence pattern of NO_x was similar to both NO and NO_2. Although emission hot spots of NO, NO_2, and NO_x are widespread in the NCP, the long-range transport of these species to Yufa is limited by the lifetime of these species. The average O_3 concentration for spring, summer, autumn, and winter was 20, 11, 32, and 42 ppb, respectively, at Yufa, and the typical lifetime of NO was 66, 51, 106, and 181 s in spring, summer, autumn, and winter, respectively, if it is assumed that all the NO is removed mainly by chemical reaction with O_3 (Burkholder et al., 2015). The transport distance of NO was therefore less than 5 km even with a high wind speed of 15 m s^{-1}. Even when considering the conversion of NO from NO_2 with a conversion efficiency of ∼ 30 % in summer and autumn (Takegawa et al., 2009), the transport distance of NO is still limited because the lifetime of NO_2 is also relatively short (Beirle et al., 2011; Gu et al., 2013). That is, NO concentration is determined by local emissions rather than regional transport. NO_2 and NO_x have longer lifetimes in the atmosphere than NO has, typically on the order of 4–5 h, and with a longer photochemical lifetime in cold seasons (Beirle et al., 2011; Gu et al., 2013). Hence, the typical transport distance of these species is around 100 km at the wind speed of 5 m s^{-1} (Beirle et al., 2011). Within such transport distance, the Yufa site is surrounded by various NO_x emission hot spots (Fig. 6), such as the megacity Beijing to the north, the Baoding–Cangzhou area to the south, and the Tianjin–Tangshan area to the east. Meanwhile the emission intensity was larger in winter and autumn than that in spring and summer (Fig. 6). It is therefore reasonable to observe the influence of short-range transport, in addition to local emissions, on the local NO_2 and NO_x concentrations, especially in cold seasons (Fig. 7c and d). Although our results suggest that short-range transport from these surrounding areas, especially the urban area of Beijing, was a non-negligible factor affecting the NO_x concentration at the Yufa site, the regional transport of NO_x was of less significance compared to SO_2 and CO due to its limited transport distance (see below).

Figure 7e is the seasonal bivariate polar plots of CO, which clearly show the relatively higher mean concentration of CO (> 1 ppm) with winds at low wind speed (< 2 m s^{-1}), similar to nitrogen oxide species. The mean concentration of CO was relatively higher with a higher wind speed (> 5 m s^{-1}) from the southern sector in spring and summer, from northeastern and southern sectors in autumn, and from northern and southern sectors in winter. The oxidation lifetime of CO is typically ∼ 20 days, under the assumption of an OH radical concentration of 2×10^6 cm^{-3} (Xu et al., 2011). This is substantially longer than the lifetime of NO_x, making regional transport of CO an important process affecting local air quality in the downwind area. The different lifetimes of CO and NO_x appeared to explain the unique high concentration of CO, but not NO_x, at wind speeds exceeding 5 m s^{-1} from the south and the east. Our results suggest that regional transport from the southern and central NCP and the Tianjin area could greatly affect local concentrations of CO at the Yufa site.

Figure 7a clearly shows the relatively higher mean concentration of SO_2 (∼ 20 ppb) with winds at higher wind speed (> 5 m s^{-1}) from the southern sector in spring and summer.

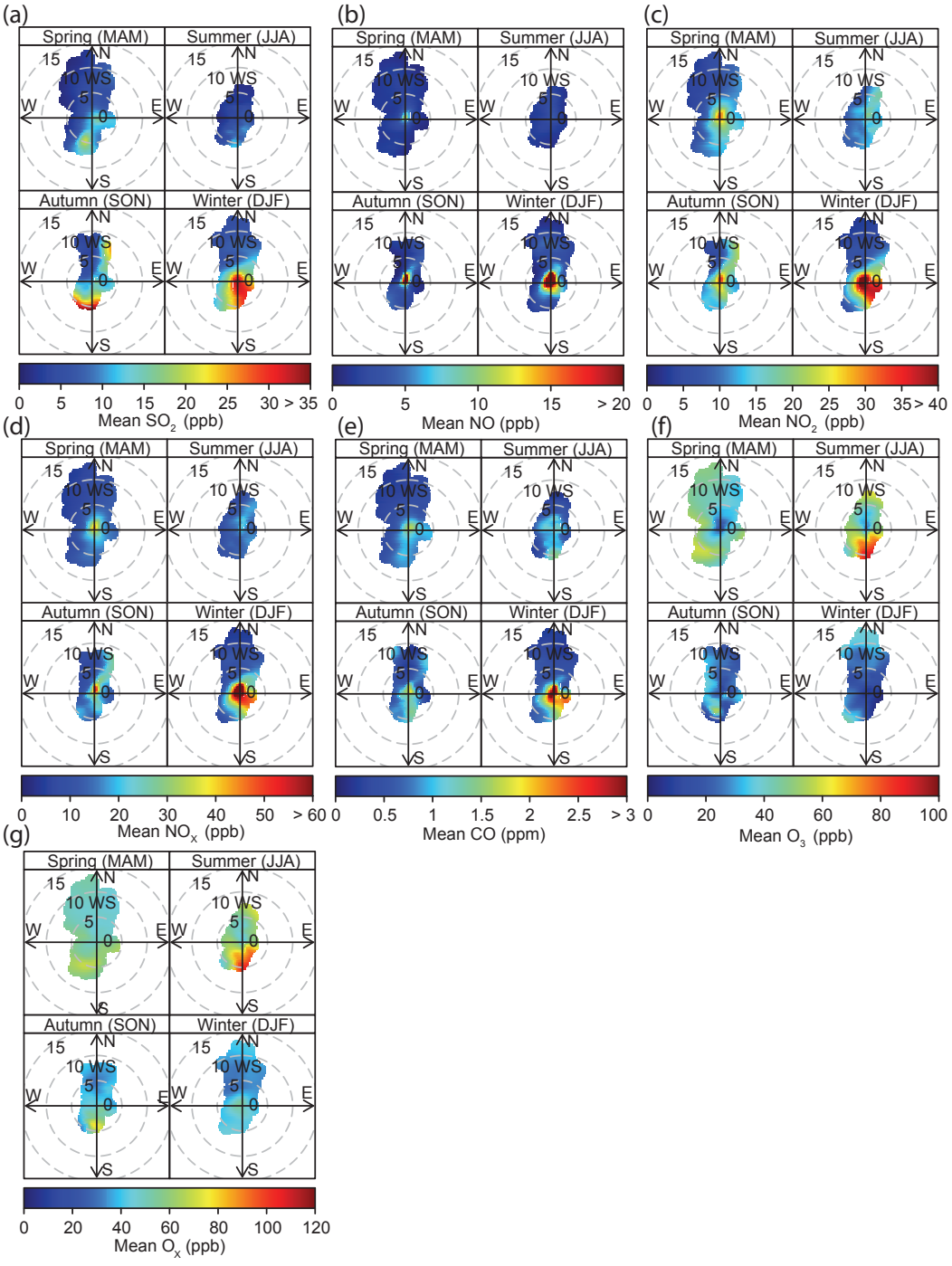

Figure 7. Seasonal bivariate polar plots for SO_2 **(a)**, NO **(b)**, NO_2 **(c)**, NO_x **(d)**, CO **(e)**, O_3 **(f)**, O_x **(g)** and concentrations based on hourly mean data at the Yufa site from 1 September 2006 to 31 August 2008. The color scale shows the concentrations of pollutants in ppb (or ppm specially for CO) and the radial scale shows the wind speed ($m\,s^{-1}$), which increases from the center of the plot radially outwards.

The mean concentration of SO_2 was high (> 30 ppb) with a higher wind speed (> 5 $m\,s^{-1}$) from the northeastern, eastern, and southern sectors in autumn and winter. Similar to CO, SO_2 has a relatively long lifetime in the atmosphere compared to NO_x, i.e., a couple of hours to 1–2 days, with longer lifetime in winter and shorter lifetime in summer (Beirle et al., 2014; He et al., 2012; Lee et.al., 2014), and regional transport of SO_2 was expected to occur. Accordingly, regional transport from emission hot spots located south of the Yufa site (Fig. 6) was found to influence the concentra-

Table 2. The total and seasonal net surface flux intensities (mean ± SD) ($\mu g\,s^{-1}\,m^{-2}$) of gaseous pollutants at the Yufa site from 1 September 2006 to 31 August 2008.

Flux ($\mu g\,s^{-1}\,m^{-2}$)	SO_2	NO	NO_2	NO_x	CO	O_3	O_x
Autumn 06	5.3 ± 79.6	−6.3 ± 27.5	−3 ± 60.2	−9.4 ± 78.9	−30 ± 2730	19.4 ± 128.8	25.9 ± 177.6
Autumn 07	6.3 ± 78.8	−6.6 ± 33.6	−3.5 ± 74.3	−10.1 ± 98.6	−60 ± 2570	10 ± 120	6.6 ± 170.3
Winter 06/07	11.8 ± 139.1	−6.9 ± 47.7	3.6 ± 105.6	−3.3 ± 142.9	350 ± 4150	−11.9 ± 127.5	−8.3 ± 188
winter 07/08	−13.1 ± 113.3	−11.5 ± 46.5	−11 ± 82.3	−22.6 ± 117.6	−550 ± 3380	−29.6 ± 143.1	−40.7 ± 191.2
Spring 07	11.3 ± 90.5	−1.9 ± 12.1	0.1 ± 71.1	−1.9 ± 78.8	50 ± 2720	3.4 ± 261.8	3.5 ± 315.5
Spring 08	13.5 ± 92	−1.8 ± 15.2	0.2 ± 76.4	−1.5 ± 87	160 ± 2630	10.7 ± 266.4	10.9 ± 321.2
Summer 07	11 ± 35.3	0.4 ± 6.7	8.4 ± 46.9	8.7 ± 51.5	600 ± 1960	71.3 ± 175.7	79.7 ± 211.4
Summer 08	5.7 ± 26.1	0.1 ± 4.9	1 ± 32.7	1.1 ± 36.6	120 ± 1540	48.1 ± 183.3	49.1 ± 207.8
Total	6.2 ± 89.5	−4.3 ± 29.5	−0.6 ± 72.3	−4.9 ± 93	70 ± 2830	14.7 ± 187.8	14.8 ± 234.9

tions of SO_2 (Fig. 7a) at Yufa in all seasons. Specifically, the highlighted emission hot spots in the central NCP and the southern NCP, which accounted for about 70 % of China's coal consumption in 10 % of China's domestic area (China Statistical Yearbook, 2008), is a major source of SO_2 in the Beijing area by regional transport (Liu et al., 2016). Furthermore, regional transport from the northeastern sector of the Yufa site, where the center of the megacity Beijing located, was also observed in autumn and winter, which indicated the increased emission of SO_2 in heating seasons.

Finally, the bivariate polar plots in Fig. 7f and g show the dependence of O_3 and O_x concentration on wind speed and wind direction by season. Low O_3 concentration (< 20 ppb) was observed at low wind speed (< 2 m s^{-1}). With the northern wind at a higher wind speed (> 5 m s^{-1}), a typical background O_3 concentration (around 50 ppb) was observed in spring and summer. With southern wind at a higher wind speed (> 5 m s^{-1}), high O_3 concentration (above 60 ppb) was observed, especially in summer. The main difference of seasonal bivariate polar plots between O_3 and O_x was that no low concentration of O_x was observed under low wind speed conditions in all seasons. The low concentration of O_3 at low wind speed may be due to the titration of O_3 by NO, which was more obvious in autumn and winter. Background O_3 levels in the northwestern wind under medium and high wind speed conditions clearly reflect the transport of background air mass to the Yufa site from locations where the emission intensities of pollutants were relatively low (Fig. 6). This was more obvious in spring when the air masses from the northwest increased (Fig. 4). In contrast, O_3 concentrations higher than background level in the southern wind under medium and high speed conditions, especially in summer, suggest accumulation of O_3 during its transport from the central NCP area or even the southern NCP area to the Yufa site. Emission intensity of O_3 precursors, such as NO_x and VOCs is high in the NCP, and the solar radiation is strong in summer, which facilitates the formation and transport of O_3 from the NCP to Beijing (Zhang et al., 2014).

In conclusion, the emissions in the Beijing area are closely related to the observed concentrations of NO, NO_2, NO_x, and CO at Yufa. Regional transport had a clear influence on the concentrations of all gaseous pollutants examined here, with the exception of NO. The emission hot spots located east, northeast, and especially south of the Yufa site determined the regional transport directions. The influence of regional transport differed among species. Regional transport of SO_2, CO, and O_3 from the central and southern NCP to the Yufa site was more important, whereas regional transport of NO_x from the NCP was less evident. Factors affecting regional transport included, but were not limited to, the atmospheric lifetime of pollutants, wind field, and local and regional emissions. As the Yufa site is a cross-boundary rural site between the megacity Beijing and the NCP, observation of transport flux there is appropriate in evaluating the regional transport influence by both the megacity Beijing and the NCP on the Yufa site.

3.3 Transport flux

To evaluate the surface transport of the main air pollutants from Beijing and the NCP to the Yufa site, the surface flux intensities were calculated with Eq. (3) based on observations at the Yufa site. The mean net surface flux intensities in each season were also calculated for the 2-year observation period (Table 2). The overall net surface flux intensities (mean ± SD) of SO_2, NO, NO_2, NO_x, O_3, O_x, and CO were 6.2 ± 89.5, −4.3 ± 29.5, −0.6 ± 72.3, −4.9 ± 93.0, 14.7 ± 187.8, 14.8 ± 234.9, and 70 ± 2830 $\mu g\,s^{-1}\,m^{-2}$ during the observation period from 1 September 2006 to 31 August 2008, respectively. The large standard deviation of the surface flux intensity indicated the large variations in the transport flux intensities. Table 3a shows the mean influx intensities (positive, from the NCP to Yufa) were highest in winter and lowest in summer, with the flux intensity values in winter 2–6 times of those in summer. The outflux intensities (negative, from Beijing to Yufa) show the same pattern, with the absolute flux intensity values in winter 2–8 times

of those in summer (Table 3b). Yet the overall net transport surface flux intensities show quite different seasonal variations (Table 2) compared to the results in Table 3. For SO_2, CO, O_3, and O_x the surface transport flux intensities from the NCP to Yufa surpassed those from Beijing to Yufa in all seasons except in winter, while the strongest net fluxes largely appeared in summer, which were about 4–8 times those of other seasons. The net surface transport flux intensity of NO_x from Beijing to Yufa was stronger than that from the NCP to Yufa except in summer, with the strongest net flux in winter, which was about 1.3–8 times that of other seasons.

To understand the transport fluxes reported here, it is necessary to discuss the affecting factors. First, the prevalent wind is a dominant factor affecting the surface fluxes. Figure 8 shows the time series of daily average surface flux intensity, i.e., the per unit cell flux ($\mu g\,s^{-1}\,m^{-2}$) of SO_2, NO, NO_2, NO_x, O_3, O_x, and CO, and corresponding wind vectors ($m\,s^{-1}$) during the observation period. In general, the variations in the pollutant flux intensities showed a saw-toothed pattern, with influx (positive, from the NCP to Yufa) and outflux (negative, from Beijing to Yufa) prevailing according to the shift in wind direction. Meanwhile, mainly due to the seasonal variations in wind speed and wind direction (Figs. 3 and 4), the magnitude of surface fluxes showed similar seasonal variation (Table 2). High net positive influx intensities were observed in summer and high net negative outflux intensities were observed in winter. As the northern wind prevailed significantly over the southern wind in winter, and the southern wind over the northern wind in summer (Fig. 4), the values of net surface flux intensities in these two seasons were the highest. During the other two seasons, frequent changes in positive and negative fluxes tended to cancel each other out, making the net transport fluxes less significant. This dominant role of wind field could also be illustrated by conditions during the winters of 2006/07 and 2007/08. Exceptionally, the southern wind prevailed in the winter of 2006/07 (Fig. 4), leading to the more positive surface flux intensity of pollutants in the winter of 2006/07 than the winter of 2007/08 (Table 2). For example, the increase of influx intensity for SO_2, NO, NO_2, NO_x and CO between the winter of 2006/07 and the winter of 2007/08 was on the order of a factor of 1.5 (Table 3a).

Second, the transport flux is determined not only by the wind field but also by the emissions of pollutants in the upwind area. Various pollutants showed different patterns of seasonal variations in flux as a result of relatively high emission intensities in the upwind area compared to local emissions. For example, the seasonal surface flux intensities of SO_2 were mainly positive influx, except in the winter of 2007/08. The significant regional transport of SO_2 from the NCP to Yufa in all seasons except winter could be partly attributed to the high emission intensity of SO_2 in the NCP (Fig. 6) and the reduction of SO_2 emission in Beijing (Qin et al., 2009; Wang et al., 2009a, 2011), whereas the SO_2 outflux from Beijing to Yufa was determined by the prevalent northern wind, as explained above. In contrast to the net positive influx of SO_2, the net seasonal surface flux intensities of CO were negative in both winter and autumn. The small outflux of CO in autumn reflected increased CO emission in Beijing, which was sufficiently strong to account for the strong CO emissions in the NCP.

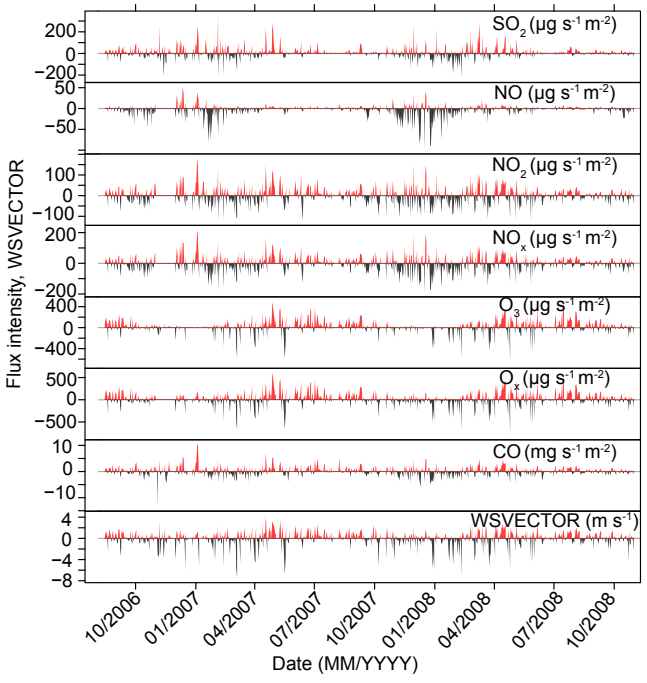

Figure 8. Time series of surface flux intensity (i.e., flux per unit cell, $\mu g\,s^{-1}\,m^{-2}$ or $mg\,s^{-1}\,m^{-2}$) for SO_2, NO, NO_2, NO_x, O_3, O_x, CO, and wind vector (i.e., $\mathrm{WSVECTOR} = -\frac{1}{n}\sum_{j=1}^{n} \mathrm{WS}_j \times \cos\theta_j$, $m\,s^{-1}$) based on daily average data at the Yufa site from 15 August 2006 to 31 October 2008. The red shaded line indicates the positive transport direction of gaseous pollutants from south to north (i.e., from the NCP to Yufa) and the black shaded line represents the negative transport direction of gaseous pollutants from north to south (i.e., from Beijing to Yufa).

The influence of emissions on transport flux could also be inferred from an emissions-reduction scenario. For example, the 29th Olympic Games were held in Beijing during the period from 8 August 2008 to 20 September 2008. The Beijing government implemented aggressive long- and short-term air quality control measures in Beijing and its surrounding areas before and during the Olympic period to maintain good air quality during the Olympic Games (Wang et al., 2010, 2011). The control measures included moving heavily polluted factories out of Beijing, reducing the traffic emission through an odd/even plate number rule, and freezing construction activities (Wang et al., 2009a). The concentrations of pollutants and the surface flux intensities during the 2008 Olympic Games were substantially reduced compared to the corresponding period of 2007 (Table 4). Besides the favored

Table 3. (a) The total and seasonal surface influx intensities (mean ± SD) (positive; from the NCP to Yufa, $\mu g\,s^{-1}\,m^{-2}$) of gaseous pollutants at the Yufa site from 1 September 2006 to 31 August 2008. (b) The total and seasonal outflux intensities (mean ± SD) (negative; from Beijing to Yufa, $\mu g\,s^{-1}\,m^{-2}$) of gaseous pollutants at the Yufa site from 1 September 2006 to 31 August 2008.

(a)							
Influx ($\mu g\,s^{-1}\,m^{-2}$)	SO_2	NO	NO_2	NO_x	CO	O_3	O_x
Autumn 06	53.3 ± 62.7	5.1 ± 7.9	42.5 ± 34.3	47.6 ± 37.9	1770 ± 1740	85 ± 131.6	143.1 ± 158.3
Autumn 07	43.9 ± 80.8	8.5 ± 14.5	48.7 ± 51.8	57.2 ± 60.7	1720 ± 1820	65.1 ± 116.8	117.3 ± 140.2
Winter 06/07	106.3 ± 126.1	19.8 ± 30	82.3 ± 83	102 ± 101.5	3360 ± 3620	40.1 ± 74.1	122.4 ± 112.8
Winter 07/08	72.3 ± 95.1	13.6 ± 20.9	60.4 ± 60.2	74 ± 72.6	2170 ± 2130	41.7 ± 70.2	102.1 ± 98.3
Spring 07	62.9 ± 88.3	3.8 ± 7.2	53.6 ± 46.6	57.5 ± 49.7	1970 ± 2050	158.8 ± 193.2	212.5 ± 223.1
Spring 08	64.7 ± 97.5	6 ± 9	56.8 ± 44.6	62.7 ± 49.1	2090 ± 1850	162.5 ± 194.4	222.9 ± 217.9
Summer 07	22.3 ± 38.7	2.9 ± 5.4	32.4 ± 30.1	35.3 ± 32.4	1560 ± 1630	140.7 ± 177.9	173.1 ± 199.7
Summer 08	18.9 ± 24.3	2.8 ± 2.6	20.8 ± 16.3	23.6 ± 18.2	1060 ± 880	138.2 ± 168.9	160.1 ± 180.2
Total	53.2 ± 84.8	7.4 ± 15.4	48.3 ± 51.5	55.8 ± 60.7	1920 ± 2130	108.2 ± 159.2	159.7 ± 180
(b)							
Outflux ($\mu g\,s^{-1}\,m^{-2}$)	SO_2	NO	NO_2	NO_x	CO	O_3	O_x
Autumn 06	−40.4 ± 66	−17.8 ± 34.4	−48.6 ± 43.9	−66.4 ± 67.3	−1830 ± 2360	−44.7 ± 87.5	−91.2 ± 103.4
Autumn 07	−30.2 ± 56.5	−21.4 ± 39.9	−54.5 ± 54.9	−75.9 ± 82.9	−1800 ± 1910	−48.9 ± 92.3	−101.5 ± 120.4
Winter 06/07	−72.8 ± 86	−30.7 ± 48.1	−66.8 ± 67.6	−97.6 ± 103.8	−2350 ± 2380	−58.4 ± 146.3	−125.2 ± 163.9
Winter 07/08	−73.9 ± 81.6	−29.5 ± 51.2	−61.9 ± 52.9	−91.3 ± 92.4	−2490 ± 2690	−480.4 ± 159.2	−142.3 ± 175.7
Spring 07	−41.3 ± 55.8	−7.8 ± 13.2	−54.6 ± 45.6	−62.4 ± 52.6	−1920 ± 1720	−155.2 ± 225	−209.8 ± 245.6
Spring 08	−38.8 ± 44.4	−9.7 ± 16.2	−57.4 ± 56.4	−67.1 ± 65.8	−1820 ± 1660	−4151.3 ± 235.8	−205.2 ± 259.7
Summer 07	−9 ± 13.3	−4.2 ± 6.5	−34.2 ± 40.8	−38.4 ± 44.9	−1110 ± 1210	−51.6 ± 76.6	−85.8 ± 102.2
Summer 08	−12.1 ± 15.8	−3.5 ± 5	−25.6 ± 30.1	−29.1 ± 33.3	−1150 ± 1320	−75.2 ± 119.5	−100.1 ± 137.1
Total	−42.8 ± 64.6	−16.7 ± 35.2	−52 ± 52.8	−68.7 ± 77.1	−1870 ± 2080	−85 ± 163.2	−137.3 ± 184.5

meteorological conditions (Fig. S2), the significant emission reduction both in the Beijing area and the NCP during the 2008 Beijing Olympic Games played a key role in the decrease of the transport flux intensities (Zhou et al., 2010).

Finally, the chemical properties of these species could also affect the flux. Take O_3 for example, although both Beijing and the NCP are regarded as emissions hot spots for O_3 precursors, the short distance between Beijing and the Yufa site may hinder the secondary formation of O_3 to some extent. Thus, the surface transport of O_3 from the NCP to Yufa was stronger than that from Beijing to Yufa, especially in summer time with a net average surface flux intensity value of about $60\,\mu g\,s^{-1}\,m^{-2}$, which is 4–9 times of that in autumn and spring (Table 2). The lifetime of the pollutants also determined the different net transport flux intensities for different species (Tables 2 and 3), with the net transport of NO, NO_2, and NO_x from Beijing to Yufa and the net transport of SO_2, CO, O_3, and O_x from the NCP to Yufa. These results are consistent with bivariate polar plots analysis mentioned above (Figs. 5 and 7).

Overall, the flux intensities are influenced by at least the wind field, emissions inventory in both the megacity Beijing and the NCP, and the chemical fates of these pollutants in the atmosphere. These observations provide insight for the analysis of projected transport flux under various emissions-reduction scenarios in the future. On the other hand, the dependence of the fluxes on these factors, which can vary, suggests that the fluxes reported here should not be compared with other reports under different conditions.

3.4 The back trajectory and PSCF analysis

The discussion above suggested that the regional transport from both Beijing and the NCP have important influence on the air quality of the Yufa site. However, both the bivariate polar plots and surface flux intensity calculation were based on the observation data at a ground measurement site. Considering the limitation of spatial representation of the Yufa site, the PSCF analysis based on the HYSPLIT-4 model was used to demonstrate the regional transport influence of the megacity Beijing and the NCP on Yufa in this section.

PSCF analysis was used in this study by combining backward trajectories and the corresponding surface transport flux intensities of pollutants. PSCF results of SO_2, NO, NO_2, NO_x, CO, O_3, and O_x in 6 h time resolution are shown in Fig. 9 for positive influx intensities (i.e., from south to north) and Fig. 10 for negative outflux intensities (i.e., from north to south). It can be seen in Fig. 9, that the higher PSCF values for most pollutants are located in the area southwest of the Yufa site, which indicates that the positive surface flux

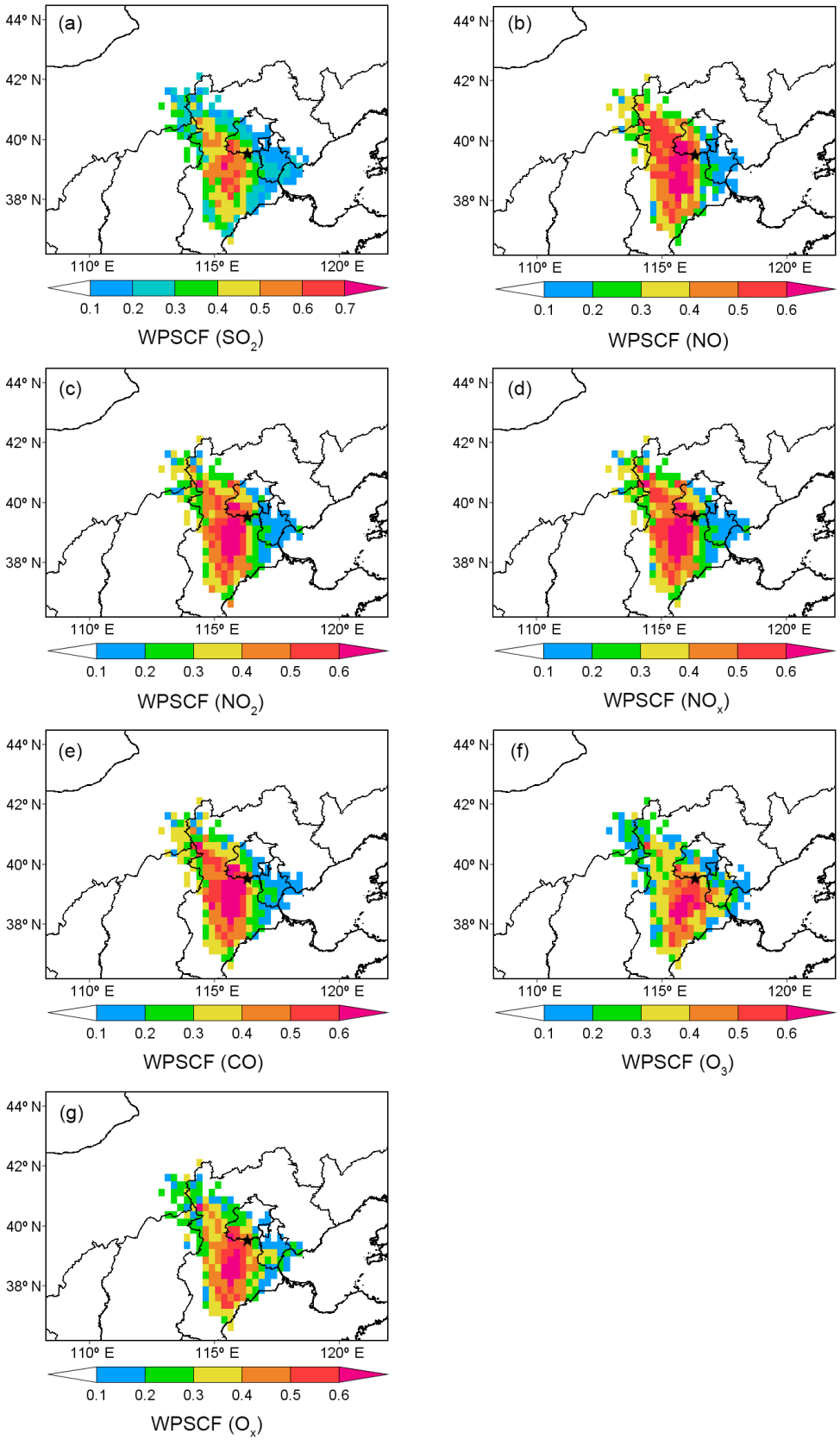

Figure 9. The PSCF maps for the SO_2 **(a)**, NO **(b)**, NO_2 **(c)**, NO_x **(d)**, O_3 **(e)**, O_x **(f)**, and CO **(g)** surface influx intensity (positive; from the NCP to Yufa). The criterion value of the surface flux intensity is set to greater than the median values, i.e., 20, 3, 30, 34, 40, 94, and 1200 $\mu g\,s^{-1}\,m^{-2}$ for SO_2, NO, NO_2, NO_x, O_3, O_x, and CO, respectively.

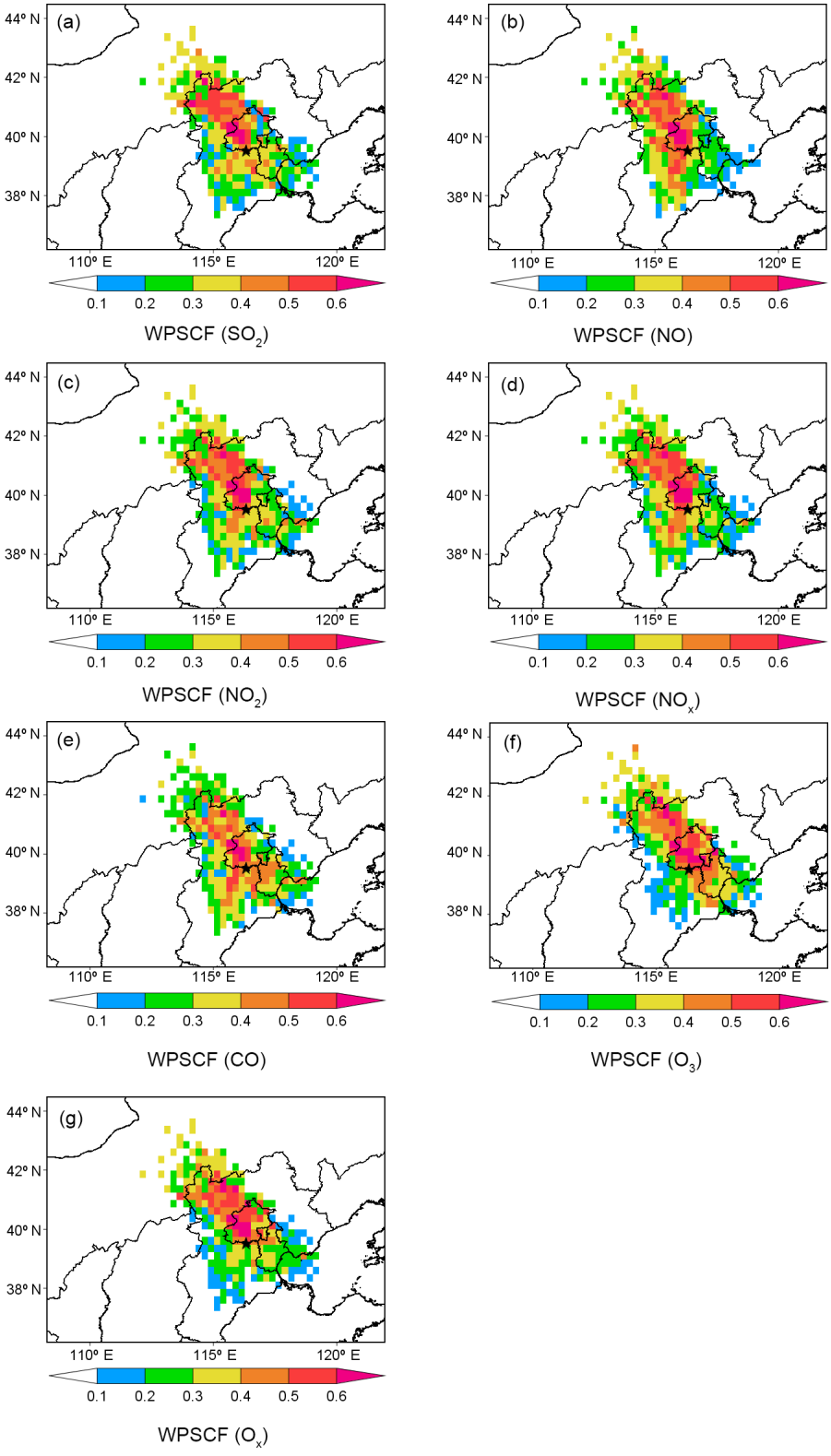

Figure 10. The PSCF maps for the SO_2 **(a)**, NO **(b)**, NO_2 **(c)**, NO_x **(d)**, O_3 **(e)**, O_x **(f)**, and CO **(g)** surface outflux intensity (negative; from Beijing to Yufa). The criterion value of the surface flux intensity is set to lower than the median values, i.e., −18, −5, −35, −43, −16, −67, and $-1200\,\mu g\,s^{-1}\,m^{-2}$ for SO_2, NO, NO_2, NO_x, O_3, O_x, and CO, respectively.

Table 4. The mean net surface flux intensities (i.e., Flux 2007 and Flux 2008), the influx intensities (positive; from the NCP to Yufa; In 2007 and In 2008), the outflux intensities (negative; from Beijing to Yufa; Out 2007 and Out 2008), and the mean concentrations (i.e., Cont. 2007 and Cont. 2008) during the 2008 Beijing Olympic period (from 8 August 2008 to 20 September 2008) and the same corresponding period of 2007 (from 8 August 2007 to 20 September 2007).

Flux ($\mu g\,s^{-1}\,m^{-2}$)	Flux 2007	In 2007	Out 2007	Flux 2008	In 2008	Out 2008	Cont. 2007 (ppb)	Cont. 2008 (ppb)
SO_2	7.9 ± 19.3	14.9 ± 20.8	-4.5 ± 4.6	1.4 ± 15.5	11.9 ± 13.6	-9 ± 8.8	3.6 ± 3.4	3.9 ± 2.2
NO	0.3 ± 8.6	3.8 ± 5	-5.9 ± 9.9	-0.1 ± 3.2	2.4 ± 1.8	-2.5 ± 2.3	4.3 ± 5.5	1.9 ± 0.6
NO_2	4.1 ± 37.9	24.1 ± 18.6	-31.3 ± 37.9	-1.3 ± 21.9	15.2 ± 11.6	-17.5 ± 17.1	16.1 ± 10.2	8.5 ± 3.6
NO_x	4.4 ± 44.5	27.8 ± 20.7	-37.2 ± 45.3	-1.4 ± 25	17.5 ± 13.2	-20 ± 19.2	20.5 ± 13.3	10.4 ± 4
CO	540 ± 158	1390 ± 1160	-980 ± 980	10 ± 1110	870 ± 670	-850 ± 740	1190 ± 490	750 ± 260
O_3	60 ± 130	117.9 ± 122.6	-42.6 ± 61.1	24.9 ± 124.6	110.9 ± 111	-60.6 ± 63.7	41.1 ± 30.5	38.9 ± 25.8
O_x	64.1 ± 154.4	141.9 ± 129.1	-73.9 ± 82.4	23.7 ± 142.1	126.7 ± 118.4	-77.7 ± 74.6	57.2 ± 27.3	47.4 ± 24.1

intensities of the Yufa site are consistent with the air masses moving from the south toward Yufa. Figure 10 shows that the higher PSCF values for most pollutants are located in the area north of the Yufa site, which indicates that the negative surface flux intensities of the Yufa site are consistent with the air masses moving from the north toward Yufa. The PSCF analysis results validate the calculated flux intensities based on observation data can be used to evaluate the regional transport influence of Beijing and the NCP on the Yufa site. However, it should be noticed that the PSCF results of NO, NO_2, and NO_x were inconsistent with the flux calculation results sometimes (Figs. 9 and 10), which may partially be ascribed to the fact that the lifetimes of these species are much shorter than 12 h. As a cross-boundary site between the megacity Beijing and the NCP, the surface flux intensities at the Yufa site may also indicate transport between the megacity Beijing and the NCP.

3.5 Uncertainty and limitation

Uncertainty in calculation of the surface flux intensities in this study mainly comes from the measurement of the pollutants and the wind. Based on the instruments used, the uncertainty of the measurement of the concentrations of SO_2, NO_x, CO, and O_3 was within 10, 10, 1, and 5 %, respectively. The uncertainty of wind speed measurement was less than 5 % and the uncertainty of wind direction was about 1 %. Thus, the uncertainty of the overall surface flux intensity for SO_2, NO_x, CO, and O_3 was less than 12, 12, 6, and 8 %, respectively.

In this study, we did not intend to extrapolate from the Yufa site to the entire region. We focus on the method developing and evaluation of the regional transport influence of Beijing and the NCP on the cross-boundary site based on the ground-based observation data. Bivariate polar plots analysis and surface flux intensity calculations were conducted, and we obtained clear evidence of surface pollutant transport from Beijing to the Yufa site and from the NCP to the Yufa site. Considering the variations in the vertical and horizontal distributions of the air pollutants and meteorological parameters, and the influence of the boundary layer on regional transport, three-dimensional observations with high precision and high resolution are needed for further comprehensive discussion of regional transport between Beijing and the NCP.

4 Conclusions

We used 2-year continuous observation data at a cross-boundary rural site between the megacity Beijing and the NCP to investigate regional transport influence on the Yufa site as part of the "Campaigns of Air Quality Research in Beijing and Surrounding Region 2006–2008" (CAREBeijing 2006–2008). The gaseous pollutants SO_2, NO, NO_2, NO_x, CO, O_3, and O_x, together with meteorological data, were determined at Yufa from August 2006 to October 2008. During the observation period, the average concentrations of the pollutants at the Yufa site were relatively high, suggesting a profound influence of the emissions from the megacity Beijing and regional transport from the NCP.

Through bivariate polar plots, we found that the southern wind, at relatively high wind speed, was essential for the inflow of SO_2, CO, and O_3 from the NCP to Yufa. For NO, NO_2, NO_x, and even CO, the emission from Beijing played a dominant role. The seasonal variations in emission intensity, meteorological conditions, and pollutant lifetimes lead to the seasonal variations in the regional transport of pollutants, hence the different bivariate polar plot patterns.

The surface flux intensities showed strong net surface transport from the NCP to Yufa in summer and net surface transport from Beijing to Yufa in winter, mainly varied with the prevailing wind. The positive net influxes of SO_2, CO, and O_3 in this study indicate a northward regional transport of these species from the NCP. In contrast, the fluxes of NO_x indicate that the influence of NO_x emission in Beijing could only influence downwind areas adjacent to Beijing, due to the limited transport distance of NO_x.

PSCF analysis demonstrated that regional transport from Beijing and the NCP to Yufa can be evaluated by the surface

flux intensity calculation based on the ground-based measurement data. As a cross-boundary site between the megacity Beijing and the NCP, the surface transport flux intensities at the Yufa site may also indicate transport between the megacity Beijing and the NCP.

Our results again suggest that Beijing and the NCP have tight interactions through regional transport of air pollutants. Factors affecting the transport flux, such as meteorological parameters, especially wind speed and wind direction, emissions inventory, and photochemical reactions, are essential for the regional transport fluxes and thus the air quality of the megacity Beijing and its surrounding areas. Therefore, both local emissions reduction and regional cooperative control should be considered in air quality management of Beijing.

5 Data availability

The observation data of the Yufa site used in this paper is available on request.

The Supplement related to this article is available online at doi:10.5194/acp-16-14265-2016-supplement.

Author contributions. Tong Zhu designed the experiments and Limin Zeng and the staff of the Yufa site carried out the experiment. Yingruo Li conducted the data analysis with contributions from all co-authors. Jun Liu provided the emission maps. Junxia Wang managed the observation data of the program. Yingruo Li prepared the paper with the help of Tong Zhu, Chunxiang Ye, Jun Liu, and Yi Zhu.

Acknowledgements. The authors express their sincere thanks to the staff of the Yufa site for carrying out the measurements. This work as part of CAREBeijing (Campaigns of Air Quality Research in Beijing and Surrounding Regions) was supported by Beijing Council of Science and Technology. This study was also supported by the National Natural Science Foundation Committee of China (21190051, 41121004, 41421064), the European 7th Framework Programme Project PURGE (265325), and the Collaborative Innovation Center for Regional Environmental Quality.

Edited by: Z. Li
Reviewed by: four anonymous referees

References

An, X., Zhu, T., Wang, Z., Li, C., and Wang, Y.: A modeling analysis of a heavy air pollution episode occurred in Beijing, Atmos. Chem. Phys., 7, 3103–3114, doi:10.5194/acp-7-3103-2007, 2007.

Ashbaugh, L. L., Malm, W. C., and Sadeh, W. Z.: A residence time probability analysis of sulfur concentrations at Grand Canyon National Park, Atmos. Environ., 19, 1263–1270, 1985.

Beirle, S., Boersma, K. F., Platt, U., Lawrence, M. G., and Wagner, T.: Megacity emissions and lifetimes of nitrogen oxides probed from space, Science, 333, 1737–1739, 2011.

Beirle, S., Hörmann, C., Penning de Vries, M., Dörner, S., Kern, C., and Wagner, T.: Estimating the volcanic emission rate and atmospheric lifetime of SO_2 from space: a case study for Kīlauea volcano, Hawaiì, Atmos. Chem. Phys., 14, 8309–8322, doi:10.5194/acp-14-8309-2014, 2014.

Burkholder J. B., Sander S. P., Abbatt J., Barker J. R., Huie R. E., Kolb C. E., Kurylo M. J., Orkin V. L., Wilmouth D. M., and Wine P. H.: Chemical Kinetics and Photochemical Data for Use in Atmospheric Studies, Evaluation No. 18, JPL Publication 15-10, Jet Propulsion Laboratory, Pasadena, http://jpldataeval.jpl.nasa.gov, 2015.

Carslaw, D. C., Beevers, S. D., Ropkins, K., and Bell, M. C.: Detecting and quantifying aircraft and other on-airport contributions to ambient nitrogen oxides in the vicinity of a large international airport, Atmos. Environ., 40, 5424–5434, 2006.

Chen, H. S., Li, J., Ge, B. Z., Yang, W. Y., Wang, Z. F., Huang, S., Wang, Y. L., Yan, P. Z., Li, J. J., and Zhu, L. L.: Modeling study of source contributions and emergency control effects during a severe haze episode over the Beijing-Tianjin-Hebei area, Science China Chemistry, 58, 1403–1415, 2015.

China Statistical Yearbook: Beijing, China Statistic Press, 2008 (in Chinese).

Gu, D., Wang, Y., Smeltzer, C., and Liu, Z.: Reduction in NO_x Emission Trends over China: Regional and Seasonal Variations, Environ. Sci. Technol., 47, 12912–12919, 2013.

Guo, S., Hu, M., Wang, Z. B., Slanina, J., and Zhao, Y. L.: Size-resolved aerosol water-soluble ionic compositions in the summer of Beijing: implication of regional secondary formation, Atmos. Chem. Phys., 10, 947–959, doi:10.5194/acp-10-947-2010, 2010.

He, H., Li, C., Loughner, C. P., Li, Z., Krotkov, N. A., Yang, K., Wang, L., Zheng, Y., Bao, X., Zhao, G., and Dickerson, R. R.: SO_2 over central China: Measurements, numerical simulations and the tropospheric sulfur budget, J. Geophys. Res.-Atmos., 117, D00K37, doi:10.1029/2011JD016473, 2012.

Henry, R. C., Chang, Y.-S., and Spiegelman, C. H.: Locating nearby sources of air pollution by nonparametric regression of atmospheric concentrations on wind direction, Atmos. Environ., 36, 2237–2244, 2002.

Jayamurugan, R., Kumaravel, B., Palanivelraja, S., and Chockalingam, M. P.: Influence of Temperature, Relative Humidity and Seasonal Variability on Ambient Air Quality in a Coastal Urban Area, Int. J. Atmos. Sci., 2013, 1–7, doi:10.1155/2013/264046, 2013.

Lee, C., Martin, R. V., van Donkelaar, A., Lee, H., Dickerson, R. R., Hains, J. C., Krotkov, N., Richter, A., Vinnikov, K., and Schwab, J. J.: SO_2 emissions and lifetimes: Estimates from inverse modeling using in situ and global, space-based (SCIAMACHY and OMI) observations, J. Geophys. Res., 116, D06304, doi:10.1029/2010jd014758, 2011.

Lin, W., Xu, X., Zhang, X., and Tang, J.: Contributions of pollutants from North China Plain to surface ozone at the Shangdianzi GAW Station, Atmos. Chem. Phys., 8, 5889–5898, doi:10.5194/acp-8-5889-2008, 2008.

Lin, W., Xu, X., Ge, B., and Zhang, X.: Characteristics of gaseous pollutants at Gucheng, a rural site southwest of Beijing, J. Geophys. Res., 114, D00G14, doi:10.1029/2008JD010339, 2009.

Lin, W., Xu, X., Ge, B., and Liu, X.: Gaseous pollutants in Beijing urban area during the heating period 2007–2008: variability, sources, meteorological, and chemical impacts, Atmos. Chem. Phys., 11, 8157–8170, doi:10.5194/acp-11-8157-2011, 2011.

Liu, J., Mauzerall, D. L., Chen, Q., Zhang, Q., Song, Y., Peng, W., Klimont, Z., Qiu, X., Zhang, S., Hu, M., Lin, W., Smith, K. R., and Zhu, T.: Air pollutant emissions from Chinese households: A major and underappreciated ambient pollution source, P. Natl. Acad. Sci. USA, 113, 7756–7761, 2016.

Matsui, H., Koike, M., Kondo, Y., Takegawa, N., Kita, K., Miyazaki, Y., Hu, M., Chang, S. Y., Blake, D. R., Fast, J. D., Zaveri, R. A., Streets, D. G., Zhang, Q., and Zhu, T.: Spatial and temporal variations of aerosols around Beijing in summer 2006: Model evaluation and source apportionment, J. Geophys. Res.-Atmos., 114, D00G13, doi:10.1029/2008JD010906, 2009.

Parrish, D. D. and Zhu, T.: Clean Air for Megacities, Science, 326, 674–675, 2009.

Qin, M., Xie, P. H., Wu, D. X., Xu, J., Si, F. Q., Wang, M. H., Dou, K., Zhang, Y., Xiao, X., Liu, W. S., Liu, S. S., Wang, F. P., Fang, W., Liu, J. G., and Liu, W. Q.: Investigation of variation characteristics and levels of SO_2-NO_2-O_3 and PM_{10} in Beijing during 2008 Olympic Games, J. Atmos. Environ. Opt., 4, 329–340, 2009.

Shao, M., Tang, X., Zhang, Y., and Li, W.: City Clusters in China: Air and Surface Water Pollution, Front. Ecol. Environ., 4, 353–361, 2006.

Streets, D. G., Fu, J. S., Jang, C. J., Hao, J., He, K., Tang, X., Zhang, Y., Wang, Z., Li, Z., Zhang, Q., Wang, L., Wang, B., and Yu, C.: Air quality during the 2008 Beijing Olympic Games, Atmos. Environ., 41, 480–492,2007.

Takegawa, N., Miyakawa, T., Kuwata, M., Kondo, Y., Zhao, Y., Han, S., Kita, K., Miyazaki, Y., Deng, Z., Xiao, R., Hu, M., van Pinxteren, D., Herrmann, H., Hofzumahaus, A., Holland, F., Wahner, A., Blake, D. R., Sugimoto, N., and Zhu, T.: Variability of submicron aerosol observed at a rural site in Beijing in the summer of 2006, J. Geophys. Res., 114, D00G05, doi:10.1029/2008jd010857, 2009.

Tang, X. Y.: The characteristics of urban air pollution in China, in Urbanization, Energy, and Air Pollution in China, Natl. Acad. Press, Washington, DC, 47–54, 2004.

Wang, M., Zhu, T., Zhang, J. P., Zhang, Q. H., Lin, W. W., Li, Y., and Wang, Z. F.: Using a mobile laboratory to characterize the distribution and transport of sulfur dioxide in and around Beijing, Atmos. Chem. Phys., 11, 11631–11645, doi:10.5194/acp-11-11631-2011, 2011.

Wang, S., Li, G. G., Gong, Z. Y., Du, L., Zhou, Q. T., Meng, X. Y., Xie, S. Y., and Zhou. L.: Spatial distribution, seasonal variation and regionalization of $PM_{2.5}$ concentrations in China, Science China Chemistry, 58, 1435–1443, 2015.

Wang, T., Ding, A., Gao, J., and Wu, W. S.: Strong ozone production in urban plumes from Beijing, China, Geophys. Res. Lett., 33, L21806, doi:10.1029/2006GL027689, 2006.

Wang, T., Nie, W., Gao, J., Xue, L. K., Gao, X. M., Wang, X. F., Qiu, J., Poon, C. N., Meinardi, S., Blake, D., Wang, S. L., Ding, A. J., Chai, F. H., Zhang, Q. Z., and Wang, W. X.: Air quality during the 2008 Beijing Olympics: secondary pollutants and regional impact, Atmos. Chem. Phys., 10, 7603–7615, doi:10.5194/acp-10-7603-2010, 2010.

Wang, M., Zhu, T., Zheng, J., Zhang, R. Y., Zhang, S. Q., Xie,X. X., Han, Y. Q., and Li, Y.: Use of a mobile laboratory to evaluate changes in on-road air pollutants during the Beijing 2008 Summer Olympics, Atmos. Chem. Phys., 9, 8247–8263, doi:10.5194/acp-9-8247-2009, 2009a.

Wang, Y. Q., Zhang, X. Y., and Draxler, R. R.: TrajStat: GIS-based software that uses various trajectory statistical analysis methods to identify potential sources from long-term air pollution measurement data, Environ. Modell. Software, 24, 938–939, 2009b.

Wehner, B., Birmili, W., Ditas, F., Wu, Z., Hu, M., Liu, X., Mao, J., Sugimoto, N., and Wiedensohler, A.: Relationships between submicrometer particulate air pollution and air mass history in Beijing, China, 2004–2006, Atmos. Chem. Phys., 8, 6155–6168, doi:10.5194/acp-8-6155-2008, 2008.

Westmoreland, E. J., Carslaw, N., Carslaw, D. C., Gillah, A., and Bates, E.: Analysis of air quality within a street canyon using statistical and dispersion modelling techniques, Atmos. Environ., 41, 9195–9205, 2007.

White, W. H., Anderson, J. A., Blumenthal, D. L., Husar, R. B., Gillani, N. V., Husar, J. D., and Wilson, W. E.: Formation and transport of secondary air pollutants: ozone and aerosols in the St. Louis urban plume, Science, 194, 187–189, 1976.

Wu, Q. Z., Wang, Z. F., Gbaguidi, A., Gao, C., Li, L. N., and Wang, W.: A numerical study of contributions to air pollution in Beijing during CAREBeijing-2006, Atmos. Chem. Phys., 11, 5997–6011, doi:10.5194/acp-11-5997-2011, 2011.

Xu, J., Ma, J. Z., Zhang, X. L., Xu, X. B., Xu, X. F., Lin, W. L., Wang, Y., Meng, W., and Ma, Z. Q.: Measurements of ozone and its precursors in Beijing during summertime: impact of urban plumes on ozone pollution in downwind rural areas, Atmos. Chem. Phys., 11, 12241–12252, doi:10.5194/acp-11-12241-2011, 2011.

Xu, X., Zhou, L., Zhou, X., Yan, P., Weng, Y., Tao, S., Mao, J., Ding, G., Bian, L., and Jhon, C.: Influencing domain of peripheral sources in the urban heavy pollution process of Beijing, Science in China, 48, 565–575, 2005.

Yuan, Z., Lau, A. K. H., Shao, M., Louie, P. K. K., Liu, S. C., and Zhu, T.: Source analysis of volatile organic compounds by positive matrix factorization in urban and rural environments in Beijing, J. Geophys. Res., 114, D00G15, doi:10.1029/2008JD011190, 2009.

Zhang, J. P., Zhu, T., Zhang, Q. H., Li, C. C., Shu, H. L., Ying, Y., Dai, Z. P., Wang, X., Liu, X. Y., Liang, A. M., Shen, H. X., and Yi, B. Q.: The impact of circulation patterns on regional transport pathways and air quality over Beijing and its surroundings, Atmos. Chem. Phys., 12, 5031–5053, doi:10.5194/acp-12-5031-2012, 2012.

Zhang, Q., Yuan, B., Shao, M., Wang, X., Lu, S., Lu, K., Wang, M., Chen, L., Chang, C. C., and Liu, S. C.: Variations of ground-level O_3 and its precursors in Beijing in summertime between 2005 and 2011, Atmos. Chem. Phys., 14, 6089–6101, doi:10.5194/acp-14-6089-2014, 2014.

Zhang, R., Jing, J., Tao, J., Hsu, S. C., Wang, G., Cao, J., Lee, C. S. L., Zhu, L., Chen, Z., Zhao, Y., and Shen, Z.: Chemical characterization and source apportionment of $PM_{2.5}$ in Beijing: seasonal perspective, Atmos. Chem. Phys., 13, 7053–7074, doi:10.5194/acp-13-7053-2013, 2013.

Zhou, Y., Wu, Y., Yang, L., Fu, L., He, K., Wang, S., Hao, J., Chen,J., and Li, C.: The impact of transportation control measures on emission reductions during the 2008 Olympic Games in Beijing, China, Atmos. Environ., 44, 285–293, 2010.

Zhu, L., Huang, X., Shi, H., Cai, X., and Song, Y.: Transport pathways and potential sources of PM_{10} in Beijing, Atmos. Environ., 45, 594–604, 2011.

Zhu, Y., Zhang, J., Wang, J., Chen, W., Han, Y., Ye, C., Li, Y., Liu, J., Zeng, L., Wu, Y., Wang, X., Wang, W., Chen, J., and Zhu, T.: Distribution and sources of air pollutants in the North China Plain based on on-road mobile measurements, Atmos. Chem. Phys., 16, 12551–12565, doi:10.5194/acp-16-12551-2016, 2016.